Investigating the Mechanism of Lithium Transport at Solid Electrolyte Interphases

Ryan Jorn[*]*, Lauren Raguette, Shaniya Peart*

Department of Chemistry, Villanova University, Villanova, Pennsylvania 19085, United States

Abstract:

Reactions between carbonate electrolytes and graphite electrodes in lithium-ion storage devices produce a surface film of byproducts known as the Solid Electrolyte Interphase (SEI). Significant progress has been made in assessing the composition and structure of these interphases, however their impact on lithium transport during charge and discharge lacks molecular detail. Over the past decade electrochemical impedance spectroscopy (EIS) has shown that lithium transport is limited by a combination of ion desolvation and ion conduction through the SEI, however which step is rate-limiting remains unresolved. In this work we simulate the first step in this process, i.e. ion desolvation, both into and out of two model SEI's comprised of lithium ethylenedicarbonate (LEDC) and Li_2CO_3 interfaced with an ethylene carbonate electrolyte. By correlating free energy changes with solvation structure, we show that the path taken for Li^+ insertion is a two-step mechanism consisting of overcoming two energy barriers to adsorption and then absorption. The largest measured barrier of the two is 59.2 kJ/mole, within the estimates obtained from EIS measurements. Ion extraction from the LEDC, however, follows a different free energy profile determined by the flexibility of the surface groups to extend into the electrolyte. The dependence of extraction from LEDC on the nature of the surface groups, emphasized by comparison with ion extraction from the more rigid Li_2CO_3 surface, highlights the complex relationship between SEI composition and lithium transport.

[*] Author to whom correspondence should be addressed: ryan.jorn@villanova.edu

I. Introduction:

Efficient shuttling of lithium ions between the electrodes of energy storage devices requires electrochemically stable and ion conductive electrolytes.[1] Regarding electrochemical stability, a continual challenge has been controlling the chemistry at the electrode surface during ion insertion and abstraction.[2] For typical mixtures of cyclic and linear carbonate solvents,[3] side reactions are prevalent upon the first charging event (and indeed in some cases occur spontaneously before charging). Such side reactions occur from competition between lithium ion transfer and the reduction or oxidation of solvent molecules and metal salt anions.[4] Over time, the reaction products build up at the electrode/electrolyte interface to form a surface film known as the Solid Electrolyte Interphase (SEI).[2] Ideally, the SEI acts to protect the electrode surface from further side reactions without impairing the flow of lithium ions to and from the electrode. However, in practice the cost for this protection is a loss of active lithium ions for charge transport (capacity fade from being stuck in the SEI)[5] and additional energy barriers to lithium migration.[6] Thus the formation of the SEI plays a critical role in the charge transport mechanism of lithium-ion systems and yet the parameters dictating its influence are not well understood.[7]

Assessing the impact of the SEI on battery operation has fueled decades of research into its chemical composition and structure.[2,8] Consensus on these topics has been difficult to achieve, in part due to the large number of experimental parameters affecting the content of the SEI (for example the nature of the electrode surface,[9] composition of the electrolyte,[10–12] salt concentration,[13–15] and exposure to moisture[16]) and the highly heterogeneous nature of its growth mechanism.[17] The SEI is known to consist of a combination of inorganic and organic species for well-studied electrolytes comprised of ethylene carbonate (EC), propylene carbonate (PC), and dimethyl carbonate (DMC) mixed with $LiPF_6$, $LiBF_4$, and $LiClO_4$. The inorganic products include

lithium oxide,[17] lithium fluoride,[9,18] and lithium carbonate,[19] but the list of candidate organic species spans dicarbonates to ether polymers.[20–22] Efforts to further elucidate the products formed during charge cycling continue to refine the picture of the SEI composition. Wang et al. recently discovered that the long-assumed major product from EC electrolytes, lithium ethylene dicarbonate (LEDC), may involve a more complex equilibrium between lithium ethylene mono-carbonate (LEMC) and lithium methyl carbonate (LMC).[23] In addition to the composition of the surface films, their growth and structure have also received significant research focus. Two models often reported are the mosaic structure in which the SEI consists of a patchwork of domains of differing composition,[24] and a layered model consisting of inorganic compounds at the electrode surface followed by organic compounds closer to the electrolyte.[25–27] Cryo-TEM studies of SEI growth suggest that both structures may arise during SEI formation, even on the same types of electrode particles in contact with the same electrolyte.[17]

Understanding the nature of the electrode/electrolyte interface allows one to connect the composition and structure of the resulting surface films with their influence on lithium transport.[28] The exchange of lithium ions between the electrolyte and SEI has been directly observed via ^{6}Li isotope labeling experiments in combination with time-of-flight secondary ion mass spectrometry[29] and NMR spectroscopy.[30] These studies demonstrate the permeability of the SEI to lithium transfer and indicate that the time scale for lithium exchange at unbiased interfaces could be on the order of seconds or minutes. These studies were not, however, able to provide a detailed exploration of the steps to ion exchange. The presence of the SEI introduces three new stages to the voyage of a lithium ion from the electrolyte to the anode.[31] First, the lithium ion must reach the SEI by transport from the bulk electrolyte. Second, the lithium must be transferred into the SEI by exchanging its solvation structure in the electrolyte for coordinating species in the film.

This process is often referred to as ion desolvation, but more accurately represents a "resolvation" since the end state is not a bare ion and the film structure may be amorphous.[32] Ion transfer from the electrolyte into the film can be achieved by the creation of a defect in the film structure (interstitial or vacancy)[33–35] or via the knock-off mechanism[36] in which the lithium replaces an ion from the existing film. The third and final step in the lithium's journey to the electrode requires traversing the SEI by defect migration, knock-off transport, or conduction along the grain boundaries separating film domains.[37,38] With an eye towards improving the rate of charge transport and battery performance, the question then becomes which of these three steps (bulk electrolyte transport, desolvation, or SEI migration) is rate limiting.

Electrochemical impedance spectroscopy (EIS) provides a tool for quantitatively studying the resistance associated with each process in lithium ion conduction.[2,39] The activation energy for lithium transport can be extracted at different stages of charge cycling by measuring the temperature dependence of the impedance spectrum.[40,41] Trends that emerge from using different combinations of electrodes and electrolytes can yield insight into which aspect of the lithium transport is rate limiting.[42–44] Mirroring the continued discussions over SEI composition and structure, general consensus has been elusive on which step is the most energetically costly. Studies have been published that support both desolvation[31,43–45] and SEI migration[6,40] as the bottle-neck to charge shuttling. Early works by Abe et al.[46] and Yamada et al.[44] indicated that for a fixed SEI grown in EC and interfaced with different electrolyte mixtures, activation energy barriers varied according to the electrolyte composition (ranging from 40-60 kJ/mole). Hence the trend supported the electrolyte-dependent desolvation process being the primary hinderance to lithium transport. However, Keefe et al. argued that the differences observed in the resistance at the cathode and anode for the same electrolyte implied the importance of the surface films over

desolvation.[40] Jow et al. also observed a distinct difference in reported activation energies at the cathode versus the anode with different SEI-forming additives.[6] In an effort to decouple lithium desolvation from SEI migration, several researchers have considered cells comprised of lithium titanate (LTO) electrodes, which do not favor SEI formation.[31] Surprisingly, the activation energy for lithium conduction through the LTO interface is reported to be within the range of values reported for graphite, that is 60 kJ/mole.[47,48] All of the cited EIS studies depend on fitting data to an equivalent circuit model and greater molecular-scale information is sorely needed in order to understand the interplay of desolvation and SEI migration. Of course, reality may be even more complex and both processes may be rate-limiting at different stages of interface evolution.[41,49]

In contrast to studies of SEI film growth,[5,50–55] few atomistic simulations have investigated lithium ion transport at the SEI/electrolyte interface.[39] The vast majority of calculations on lithium ion migration have simulated transport through pure components of the SEI from perfectly crystalline lithium salts,[34–36,56] to grain boundaries between pure phases,[37] and finally amorphous dicarbonate structures.[57–60] From these works, only Borodin and Bedrov discussed the rate of lithium exchange at the SEI/electrolyte interface in an EC/DMC solvent and calculated the activation energy for lithium transfer to be around 0.42eV. The reported energy barrier to lithium desolvation was much smaller than their previously calculated barrier to migration through LEDC (0.66 eV). Going beyond classical molecular dynamics, Li and Qi developed a density functional theory tight binding (DFTB) model for lithium electrolytes and studied the migration of lithium ions from an EC electrolyte through a thin layer of crystalline Li_2CO_3 on a lithium metal electrode.[61] The barrier to adsorption onto the lithium carbonate crystal was reported to be 0.49eV, followed by a much larger energy cost for lithium insertion and migration in the crystal film (0.86 eV at 0V with respect to Li^+/Li^0). Both Borodin and Bedrov and the work of Li and Qi concluded

that the SEI migration likely presents the highest barrier to lithium transport. On the other hand, several reports have also considered the desolvation of lithium at clean graphite surfaces using classical molecular dynamics,[62] hybrid quantum/classical dynamics simulations,[63] and combinations of density functional theory (DFT) with the effective screening medium approach to account for applied voltage.[64] The results from these works show similar voltage-dependent energy barriers ranging from 0.4 – 0.73eV for desolvation. These estimates agree with those found for lithium ions at a cathode surface comprised of $LiFePO_4$ and point to the difficulty in detangling the contributions from SEI migration and desolvation based on activation energy alone.[65]

While previous work has been successful in matching energy barriers reported by EIS experiments, our present work takes a deeper look at the mechanism of lithium transfer at aged SEI/electrolyte interfaces. In specific, we apply classical molecular dynamics with umbrella sampling to investigate the first two steps of lithium transport at both disordered and crystalline interfaces: transport from the bulk electrolyte and resolvation at the film surface. From the outset our effort is not capable of resolving the question of whether interfacial energy barriers are larger than SEI diffusion barriers. However, by considering two different types of SEI, we hope to explore the impact of different surface groups on charge transfer barriers and estimate their size. Since we consider aged interfaces separated from the graphite electrode surface by a thick SEI, the role of applied electric fields is not considered explicitly.[66] Encouragingly, we find our estimated free energies for transfer agree with the reports summarized above and at the same time yield new insights by analyzing the pathways taken by the lithium ions with respect to a simple collective variable. In particular we identify two modes of ion exchange, one in which lithium are transferred between average solvation structures and a second dependent on the interpenetration of the SEI oligomers into the electrolyte solvent.

II. Method:

The aged solid electrolyte interphase (SEI) was modeled as a film of either disordered lithium ethylene dicarbonate (LEDC) or a crystal of Li_2CO_3 (see Figure 1 for structures). While recent reports have cast doubt on the importance of LEDC to SEI composition,[23] it never-the-less provides a useful test case for contrasting the effect of a flexible carbonate binding group with a relatively frozen interface, as discussed below. Both SEI materials were placed in contact with an electrolyte consisting of ethylene carbonate and 1.3M $LiPF_6$. A higher initial salt concentration was employed for the lithium hexaflurophosphate in order to offset the lithium and PF_6^- accumulation at the SEI boundary during the simulation. The bulk concentration after equilibration is comparable to the 1.0M concentration used in previous studies. The inter- and intramolecular forces in the EC-based electrolyte were described using a previously tailored model,[66] while the LEDC and Li_2CO_3 were described using the CFF91 force field and point charges determined from RESP fitting.[32] The electrostatic interactions between atoms and their periodic images were included via PPPM in the LAMMPS software package.[67] The simulation cells were created by random packing of the electrolyte region, via Packmol,[68] with dimensions of 40 Å x 40 Å x 80 Å for the amorphous LEDC and 33.435 Å x 40.639 Å x 80 Å for the Li_2CO_3 film. The electrolyte box for the Li_2CO_3 was designed to hold an integer number of crystal unit cells with the [010] plane facing the electrolyte.[32,34] The SEI region of both types of simulation cells were chosen to be half as thick in the z direction as the electrolyte region (i.e. 40 Å). The LEDC film was constructed by random packing of the SEI slab while the Li_2CO_3 film was constructed to be perfectly crystalline prior to relaxation.

After random packing of the electrolyte, the initial configurations were relaxed by the same simulated annealing procedure used in a previous study.[32] The LEDC was heated to 900K, well

past its melting point using the present model, allowed to evolve for 5 nanoseconds, and finally cooled to 453K over a period of an additional 2 nanoseconds. The electrolyte remained frozen during this phase of the SEI equilibration and a time step of 1 femtosecond was used throughout. The equations of motion during the annealing process included a Nosé-Hoover thermostat under constant volume conditions. Once returned to 453K, the entire system (SEI+electrolyte) was allowed to equilibrate for 5 nanoseconds at 1 atm of applied pressure by using a Nosé-Hoover thermostat and barostat. For simulations involving the Li_2CO_3 films, the electrolyte was annealed first with a frozen film surface. After electrolyte annealing, the top three layers of the lithium carbonate crystal were allowed to relax over an additional 3 ns. Equilibration of the simulation cell and the subsequent constrained dynamics were performed using the LAMMPS[67] molecular dynamics engine with the Colvars package.[69]

After annealing and equilibration, the final configurations of the SEI and electrolyte were used to launch umbrella sampling windows to explore lithium transport. The collective variable used during the umbrella sampling is denoted Z_{Li} and corresponds to the distance between a selected lithium ion and the xy-plane dividing the center of the SEI, see Figure 2. Three separate umbrella sampling paths were traced out in these simulations: the first followed a single lithium ion initially in the electrolyte and inserted into the LEDC film (Path 1), the second followed a lithium ion that was extracted from the LEDC to the bulk electrolyte (Path 2), and the third followed a similar course to Path 2 but with a lithium from the Li_2CO_3 film transferred to the bulk electrolyte region. Each path started from a single configuration that spawned the first seven umbrella sampling windows by introducing a moving bias potential to pull the target lithium ion to a given value of Z_{Li} over 500 picoseconds. Once the lithium was pulled to the correct position, the system was equilibrated for another 2.5 nanoseconds. For subsequent umbrella sampling

simulations, the endpoint from the equilibration of the previous window was used as the starting point for the next window in order to maintain consistency with paths of entry/exit to the film surface. In each window the collective variable was constrained by a harmonic potential with centers separated from neighboring windows by 0.25-0.75 Å and force constants ranging from 10-100 kcal/(mole $\cdot$ Å^2). The larger force constants were found necessary when the ion was exchanged at the SEI film surface and an additional restraining force was applied to the SEI center-of-mass to prevent moving the entire film. The value of the collective variable was recorded at 20 femtosecond intervals to provide sufficient data to build histograms for the free energy calculation (see Supporting Information for histograms). Each window simulation was propagated for 30 nanoseconds to obtain converged solvation structures for the constrained lithium. Finally, the freely available WHAM package, distributed by the Grossfield lab,[70] was used to obtain the free energy curves with respect to Z_{Li} and Monte Carlo bootstrapping was used to estimate error bars. Correlation times were assessed by integrating the autocorrelation function for the collective variable. As discussed subsequently, the first two paths showed significant differences in spite of similar endpoints and illustrate the dependence of ion exchange at the SEI on surface group/electrolyte mixing.

III. Results and Discussion:

A. Ion Solvation Structure and Transfer Mechanisms

Free energy curves for lithium ion insertion into LEDC (Path 1) and accompanying changes in solvation structure are shown in Figure 3 and Figures S7–S8 in the Supporting Information. Given the rugged nature of the SEI/electrolyte interface, the position of the film surface was determined by the intersection between the LEDC and EC center-of-mass densities (see Figure S1 from Supporting Information for the graph of densities). When plotted together, the free energy

and coordination show a clear correspondence between transitions in solvation structures and energy barriers to ion exchange. Starting far from the film and approaching the surface, one can see changes in EC coordination that were previously correlated with the diffuse, adsorbed, and absorbed regions of the lithium density profile.[32] These labels are defined as follows: diffuse refers to the region with EC coordination between 2.15 and 4.3 molecules (i.e. from half of the bulk electrolyte solvation shell to full bulk solvation), adsorbed refers to the region with EC coordination between 1.0 and 2.15 molecules (i.e. from a single EC to half of the bulk electrolyte solvation shell), and finally absorbed refers to the region with EC coordination by less than 1 molecule. Starting from the bulk electrolyte coordination number of 4.3 EC molecules, Figures 3 and 4 show that the average number of solvating EC molecules decreases slightly to 3.65 as the lithium moves from 13 Å to 3 Å with respect to the LEDC surface. The decline in EC coordination in the diffuse region agrees with DFTB calculations from Qi and Li that showed weakening of the solvation sheath even at 10 Å from a Li_2CO_3 film.[61] However, in the present case the weakening of the EC binding also comes at a gain in PF_6^- coordination.

Moving closer toward the surface film, the loss of half of the solvation shell from the bulk indicates that between 2 and 3 Å is the dividing line between the adsorbed lithium ion species and the diffuse/bulk regions of the lithium density profile. The trend in greater anion coordination seen in the diffuse region continues into the adsorbed layer: two EC carbonyl oxygens are lost with respect to the bulk solvation shell and replaced by a fewer number of LEDC carbonate oxygens (1.2–1.5). The difference in oxygen coordination is made up for by greater binding to PF_6^-. Increased contact ion pair formation at the SEI surface was noted in our previous study[32] and can be seen in Figure 4 where the phosphorous coordination climbs from 0.3 in the bulk electrolyte to 0.9 at the SEI surface.

Figure 4 shows a comparison of the coordination curves for the individually constrained lithium ion and averages across all the lithium in the simulation box within 2 Å bins. The behavior of the solvation shell composition as a function of distance from the film is consistent across all of the independent umbrella sampling simulations (representative examples from the 40 windows are shown as light lines in Figure 4). Regarding the mechanism for lithium transport, the agreement between coordination for the constrained ion and all the remaining ions at similar Z_{Li} values suggests that Path 1 is mediated by transitions between average structures from the diffuse, adsorbed, and absorbed regions. This interpretation is also supported by integrating the lithium ion density, see Supporting Information, across the liquid electrolyte region for each umbrella sampling window along Path 1. The total number of lithium ions found in the electrolyte does not change from the start to the finish of the path, which means that the biased lithium must be replaced as it moves across the concentration profile, see Figure S5 from the Supporting Information.

For each exchange of the biased lithium ion between solvation structures (Path 1), there is an accompanying energetic cost that agrees with literature values obtained from impedance spectroscopy.[6,44] The transition from the diffuse to the adsorbed solvation structure is accompanied by a free energy barrier of 42.4 kJ/mole in Figure 3, followed by a deep energy well at the SEI surface. The local minimum in free energy at the surface agrees with the tendency for ion accumulation seen in our previous studies.[32] The subsequent transfer of the lithium from the adsorbed layer into the SEI is evidenced by the drop to 0 in EC coordination and the presence of another minimum in the free energy. The adsorbed minimum is separated from the absorbed minimum, located at -1.34 Å, by a barrier height of 59.2 kJ/mole. While a larger value than the adsorbed transition, this value still lies within the range of estimated barriers from impedance spectroscopy. In total, the combination of free energy profile and solvation structure provides a

clear picture for ion exchange at the SEI surface along Path 1. The lithium is transferred from the diffuse region to the adsorbed layer and subsequently absorbed via two energy barriers of comparable magnitude (40-60 kJ/mole). The reproducibility of this transport mechanism is supported by additional umbrella sampling using other uncorrelated lithium ions, see Figure S7 and S8 in the Supporting Information. In both cases, similar features are seen: a barrier to adsorption followed by a minima at the surface and another energy barrier to absorption. However it should be noted that there was a significant spread in calculated barrier heights to adsorption (15-42 kJ/mole) from these three PMF curves. These deficiencies of brute force umbrella sampling are discussed in greater detail in Section B. While agreement with barrier heights from EIS experiments are encouraging,[6] it should also be noted that a clear link to these simulations cannot be made as a result of several factors: the molecular structure at the interface is unknown in the experiments involving graphite particles, the measured barrier height from experiment often represents a convolution of diffusion through the SEI layer as well as desolvation from the electrolyte, and the experiments reflect a system out of equilibrium while our simulations lack concentration gradients and applied electric fields. Never-the-less the agreement on estimated barrier heights is encouraging for our selection of a relatively simple force field. In comparing with other simulations, we note that similar double-barrier energy profiles to Figures 3, S7, and S8 were obtained for DFT studies of lithium ion transfer at the $LiFePO_4$ cathode.[65]

The energetics and solvation structures for ion insertion (Path 1) into the SEI are very different from those that accompany ion extraction (Path 2) from the SEI. Figure 5 shows the free energy curve for extraction with concomitant changes to the solvation structure. Clearly, the lithium starts in the absorbed region of the SEI (-2.0 Å with respect to the film surface) and experiences its first structural transition as it moves to the LEDC surface over the first two

Angstroms of Path 2. Considering the solvation structure, the EC coordination jumps from less than one (the definition of absorbed from our previous work) to about 2 molecules at 0 Å which also indicates that the ion has moved to the adsorbed layer. However, once the ion migrates to the SEI surface, its solvation behavior deviates significantly from Path 1. The lithium retains a similar EC coordination over the next 6 Å and does not see another sudden change until the bulk EC coordination is recovered around 8 Å from the film. Further insights into this transition can be found by comparing the solvation structure for the constrained lithium ion to the average across all lithium, as done for Path 1 (see Figure 6).

Figure 6 contrasts the coordination of lithium ions in representative simulations along Path 2 and shows a much longer "adsorbed" region for the constrained lithium than the unbiased cations. The extension of adsorbed-like coordination is readily connected to deformations in the SEI structure upon extraction. As confirmed visually by snapshots of the trajectories (see Figure 5), the persistence of LEDC coordination results from pulling the bound EDC^{2-} along with the constrained lithium. As the lithium is pulled, the carbonate group and the ethyl backbone of EDC^{2-} rotate and extend to allow the lithium to reach into the electrolyte. The attachment of the lithium to the carbonate from the EDC^{2-} is eventually severed once the cost of further extension of the SEI molecule becomes prohibitive. At around 7 Å from the surface, the EDC^{2-} releases the constrained lithium and retreats back to the SEI film. The return of the system to the original distributions of lithium ions in the SEI and electrolyte is confirmed by integrating the lithium ion densities in the liquid electrolyte at the start and end of Path 2, see Figure S5 in the Supporting Information. Based on these observations from the solvation structure, it is clear that Path 2 indicates a different mechanism for lithium ion exchange that involves the surface groups penetrating the electrolyte. The mechanism still involves two phases, as evidenced by the changes in solvation structure shown

in Figure 6, however these do not follow the concerted transitions found along Path 1 where the lithium is exchanged between one layer and the next in the averaged lithium density profile. In the first phase of Path 2, the lithium ion is pulled to the surface at a cost of 20 kJ/mole followed by a second phase which is determined by the cost of pulling the EDC^{2-} out of the film to form a protrusion with the lithium ion attached at its tip. The subsequent gradual 25 kJ/mole rise in free energy across the next 7 Å is related to the cost of stretching the EDC^{2-} until the constrained lithium dissociates and the bulk solvation shell is recovered. The final few angstroms of the free energy curve are relatively flat, indicating that the energy gain from the retreat of the LEDC back into the SEI offsets the energy required to detach the lithium and resolvate it with EC molecules. The qualitative differences of Path 1 and Path 2 are an important result of this work with clear implications for understanding the mechanism of charge transfer at SEI's. The ability for the surface groups to attach to lithium ions in the electrolyte, rather than the ions transitioning between solvation structures, implies that tailoring the groups present in the SEI could impact the rate of transfer. Indeed, the different mechanisms for Paths 1 and 2 may also play a role in the noted differences between discharge and charge cycles in SEI evolution and observed differences in charge transport behavior of compact inorganic and porous organic layers.[71,72] The flexibility of the surface groups provides a path for ion conduction that can lower the overall free energy difference between the bulk SEI and bulk electrolyte (Figure 5), hence future exploration of ion transfer pathways at the SEI should account for the role of solvent-surface group interdigitation when oligomers are present.

To further assess the observed differences between Paths 1 and 2, a final case was considered for extraction of a lithium from the more rigid lithium carbonate crystal surface. In contrast to our previous studies with frozen films of lithium carbonate,[32] the first three layers of

crystal film were allowed to relax during the final equilibration while the remainder of the crystal was frozen in its bulk structure. When comparing Figure 7 with Paths 1 and 2 from the LEDC surface, it is evident that the energetics and solvation structures more closely resemble the curve for insertion into LEDC along Path 1. Figure 7 shows a very small well located around 1.35 Å from the crystal surface, at roughly the same distance as seen for the adsorbed well along Path 1 for LEDC. The free energy differences separating the absorbed minimum and the adsorbed well are also very similar in both cases, around 40 kJ/mole. The total change in free energy between the absorbed and bulk electrolyte species is around 72 kJ/mole for both Figure 7 and Figure 3. Regarding the transition from the adsorbed to the diffuse region, the total change in free energy and barrier height are also closely aligned between Figures 7 and 3. These similarities suggest that the transition from the bulk/diffuse electrolyte region to the adsorbed region may be less sensitive to the details of the SEI. However, since both of the films used in this study consisted of molecules with carbonate moieties the generality of this observation is unclear. As shown by Figure 8, the coordination changes for the lithium leaving the carbonate crystal agree with averages taken across all lithium in the layers surrounding the SEI surface. The integrated lithium ion densities in the liquid electrolyte region of the first and last windows also suggest exchange of the lithium between layers since the distributions do not indicate net transfer of a lithium, see Figure S6 in the Supporting Information. As a result, the mechanism for transfer appears to align with the pathway explored earlier for ion insertion into LEDC: exchange of the lithium ion between average solvation structures corresponding to absorbed, adsorbed, and diffuse solvation structures.

While the overall mechanisms are similar for ion insertion into LEDC and extraction from Li_2CO_3, differences in the free energy curves are also notable. An obvious difference between Figure 3 and Figure 7, is the lack of a large barrier separating the absorbed and adsorbed regions.

A possible explanation for the lack of a large barrier in Figure 7 is the differences in ion accumulation at the interfaces and the extent of ion pairing. In the case of lithium carbonate, a larger amount of lithium salts from the electrolyte tend to collect by the film surface within our model[32] and, as shown in Figure 8, contact ion pairs and aggregates of salts are more prevalent at the carbonate crystal than at the LEDC film. In the case of the carbonate crystal, the lithium is nearly equally bound to all three components at the surface (EC, CO_3^{2-}, and PF_6^-) with around 1.5 of each coordinating to the biased ion. Hence the transition from absorbed to adsorbed does not require as great a structural change as seen in the case of LEDC where 2 EC molecules are shed in the process. The movement of lithium ions from the carbonate film is more dependent on the transition from the adsorbed to diffuse layers and aligns with the idea of the "desolvation" step (albeit in reverse in this case) discussed in the literature.[6,61] The adsorption barrier seen in Figure 7 does fit with estimates from Figures S7–S8, so it is also possible that Figure 3 simply captures an energetically unfavorable path due to the limitations of umbrella sampling as discussed subsequently.

In regards to all of our discussion on the energetics of solvation changes, it should be admitted that the pairwise model employed does over-structure the EC surrounding the lithium and hence the larger barrier seen in Figure 2 may be exaggerated by the over estimation of EC coordination.[66,73] However, what is clear from comparing Figures 5 and 7 is that the flexibility of the surface groups and their ability to penetrate the electrolyte play an important role in the charge transfer pathway. These results also show that the barriers separating the diffuse, adsorbed, and absorbed structures can also be modified by the composition of the SEI, even if total changes in free energy are similar.

B. Electrolyte Dynamics and Sampling Limitations

The changes in solvation structure seen as ions approach the interface are matched by changes in electrolyte dynamics. While previous work showed this trend for averages across the layers of the lithium density profile, the individually biased lithium simulations reveal very similar behavior. One metric used to assess the motion in the electrolyte is the solvation residence time defined by the solvation correlation function, $\langle H_{solv}(0)H_{solv}(t)\rangle$, for EC molecules bound to a lithium ion. The function $H_{solv}(t)$ takes on the value of 1 if the EC molecule is within the first solvation shell of lithium (taken to be 3 Å from the lithium) and 0 otherwise. By averaging the correlation function across the entire simulation, an exponential decay is observed and fitted with a stretched exponential to extract the average residence time for attachment of an EC molecule. Figure 9 demonstrates the orders of magnitude difference in solvation residence time for lithium ions embedded in the SEI film (black dashed curves) versus those found floating freely in the bulk electrolyte (blue dashed curves) region. Agreement between the correlation function for the constrained lithium and the averages across the window simulations for Path 1 (see Figure 9(a)) shows that the residence times for the constrained ion do not differ. This agreement coincides with the similarities in Figure 4 between average solvation structures and those of the biased lithium. The difference in solvation behavior seen for Path 2 is reflected in a factor of two longer residence times seen in Figure 9(b) as the ion moves to the adsorbed and diffuse regions. The slight slow-down of EC solvation is presumably related to the extended binding of the lithium by EDC^{2-} which constrains its motion and blocks other EC molecules from coordinating. Given the orders of magnitude differences seen between residence times for the adsorbed lithium (red curve), absorbed lithium (black curves), and diffuse/bulk electrolyte lithium (blue curves), proximity to the interface dominates the electrolyte dynamics rather than the differences between solvation in Path 1 and Path 2.

The slow-down seen for EC solvation residence times for the constrained ions also corresponds to changes in their ability to diffuse in the plane parallel to the SEI surface. The slowing down of lithium diffusion explains the behavior of the error bars seen in Figures 3, 5, and 7. In all cases the uncertainty in the diffuse regions is larger than the adsorbed and absorbed as a result of the differences in lithium mobility. Since only Z_{Li} is fixed for the biased ion, it should be able wander more freely in the xy plane at the fixed distance from the surface. The ability for the constrained lithium to explore the xy plane is in fact very important given the potentially heterogenous nature of the SEI film[37]. Figure 10 shows the trajectory for the biased lithium from Figure 3 as a function of distance from the surface. Clearly, as the lithium gets closer to the surface (going from panel (a) to panel (d)) the lithium is less and less able to explore the surface morphology on the time scales considered. Hence the lack of agreement between Path 1 and 2 may be, in part, a result of a sampling issue in that the lithium is unable to see the EDC^{2-} moieties protruding out of the surface as it approaches. Finally, the energy barrier to EDC^{2-} extension into the electrolyte may not be adequately sampled for the simple collective variable considered and our equilibration procedure may artificially discourage intermingling of the LEDC with electrolyte. The confinement of the lithium as it approaches the surface along with the different mechanisms for charge transport found for Paths 1 and 2 at LEDC reinforces the need for proper exploration of the role of surface group coordination in future work to describe charge transfer at these heterogeneous interfaces.

IV. Conclusions:

In this work, we have explored the connection between the structure/composition of the surface films formed in lithium-ion energy storage devices with the aid of molecular simulations. Through a variety of free energy calculations, we have considered transitions between different solvation

structures at the interface, namely the dynamics associated with ion adsorption and absorption into the surface film from the bulk electrolyte. By correlating changes in free energy with solvation structures, we have shown that two pathways exist for lithium transfer at the LEDC surface: one involving migration between average solvation structures (Path 1) and a second involving deformation of the film surface by the LEDC carbonate groups extending from the film to facilitate the exchange of lithium ions (Path 2). Examination of ion extraction from a Li_2CO_3 crystal showed greater similarity to ion insertion at LEDC, in agreement with the minimal role of carbonate group deformation in both cases. Calculated free energy barriers to absorption fall within the range previously reported from impedance spectroscopy at graphite surfaces (40-60 kJ/mole). By performing molecular simulations, greater insight is provided into the relative weights of the transitions in solvation structure during ion exchange which could prove useful in assessing the utility of certain moieties for tailoring battery properties. While this work does not provide a definitive answer to the question of whether interfacial charge transfer dominates over SEI diffusion, future work will extend these studies to compare these energy barriers to diffusion in the SEI film. Future work must also consider coordination of the surface groups in the free energy sampling and account for limitations in sampling as a function of distance from the film interface. Regarding the latter point, alternative enhanced sampling methods and higher dimensional collective variables are warranted.

V. Supporting Information: The density plots for Li^+, EC, EDC^{2-}, and PF_6^- from simulations along Path 1(Figure S1) and histograms for all three free energy curves (Figure S2-S4). Integrated Lithium ion densities to suppor the lithium exchange interpreations (Figures S5-S6) and additional PMF curves for Path 1 (Figures S7-S8).

VI. Acknowledgements: This work was supported by funding from the Chemical Theory, Modeling, and Computation division of the National Science Foundation (NSF-CHE 1900423). LR and SP also thank Villanova University for summer funding in support of this research.

VII. References:

(1) Placke, T.; Kloepsch, R.; Dühnen, S.; Winter, M. Lithium Ion , Lithium Metal , and Alternative Rechargeable Battery Technologies : The Odyssey for High Energy Density. *J. Solid State Electrochem.* **2017**, *21*, 1939–1964.

(2) Xu, K. Electrolytes and Interphases in Li-Ion Batteries and Beyond. *Chem. Rev.* **2014**, *114* (23), 11503–11618.

(3) Kasnatscheew, J.; Wagner, R.; Winter, M.; Cekic-Laskovic, I. Interfaces and Materials in Lithium Ion Batteries : Challenges for Theoretical Electrochemistry. *Top. Curr. Chem.* **2018**, *376* (16), 1–29.

(4) Borodin, O. Challenges with Prediction of Battery Electrolyte Electrochemical Stability Window and Guiding the Electrode – Electrolyte Stabilization. *Curr. Opin. Electrochem.* **2019**, *13*, 86–93.

(5) Single, F.; Latz, A.; Horstmann, B. Identifying the Mechanism of Continued Growth of the Solid – Electrolyte Interphase. *ChemSusChem* **2018**, *11*, 1950–1955.

(6) Jow, T. R.; Delp, S. A.; Allen, J. L.; Jones, J.; Smart, M. C. Factors Limiting Li + Charge Transfer Kinetics in Li-Ion Batteries. *J. Electrochem. Soc.* **2018**, *165* (2), A361–A367.

(7) Gauthier, M.; Carney, T. J.; Grimaud, A.; Giordano, L.; Pour, N.; Chang, H.-H.; Fenning, D. P.; Lux, S. F.; Paschos, O.; Bauer, C.; et al. Electrode-Electrolyte Interface in Li-Ion Batteries: Current Understanding and New Insights. *J. Phys. Chem. Lett.* **2015**, *6* (22), 4653–4672.

(8) Tripathi, A. M.; Su, W.-N.; Hwang, B. J. In Situ Analytical Techniques for Battery Interface Analysis. *Chem. Soc. Rev.* **2018**, *47*, 736–851.

(9) Liu, T.; Lin, L.; Bi, X.; Tian, L.; Yang, K.; Liu, J.; Li, M.; Chen, Z.; Lu, J.; Amine, K.; et al. In Situ Quantification of Interphasial Chemistry in Li-Ion Battery. *Nat. Nanotechnol.* **2019**, *14*, 50–56.

(10) von Wald Cresce, A.; Borodin, O.; Xu, K. Correlating Li + Solvation Sheath Structure with Interphasial Chemistry on Graphite. *J. Phys. Chem. C* **2012**, *116* (50), 26111–26117.

(11) Nie, M.; Lucht, B. L. Role of Lithium Salt on Solid Electrolyte Interface (SEI) Formation and Structure in Lithium Ion Batteries. *J. Electrochem. Soc.* **2014**, *161* (6), A1001–A1006.

(12) Yoon, T.; Chapman, N.; Seo, D. M.; Lucht, B. L. Lithium Salt Effects on Silicon Electrode Performance and Solid Electrolyte Interphase (SEI) Structure, Role of Solution Structure on SEI Formation. *J. Electrochem. Soc.* **2017**, *164* (9), A2082–A2088.

(13) Nie, M.; Abraham, D. P.; Seo, D. M.; Chen, Y.; Bose, A.; Lucht, B. L. Role of Solution Structure in Solid Electrolyte Interphase Formation on Graphite with LiPF6 in Propylene Carbonate. *J. Phys. Chem. C* **2013**, *117* (48), 25381–25389.

(14) Ming, J.; Cao, Z.; Wahyudi, W.; Li, M.; Kumar, P.; Wu, Y.; Hwang, J. Y.; Hedhili, M. N.; Cavallo, L.; Sun, Y. K.; et al. New Insights on Graphite Anode Stability in Rechargeable Batteries: Li Ion Coordination Structures Prevail over Solid Electrolyte Interphases. *ACS Energy Lett.* **2018**, *3* (2), 335–340.

(15) Wan, C.; Xu, S.; Hu, M. Y.; Cao, R.; Qian, J.; Qin, Z.; Liu, J.; Mueller, K. T.; Zhang, J.; Hu, J. Z. Multinuclear NMR Study of the Solid Electrolyte Interface Formed in Lithium Metal Batteries. *ACS Appl. Mater. Interfaces* **2017**, *9* (17), 14741–14748.

(16) Schechter, A.; Aurbach, D.; Cohen, H. X-Ray Photoelectron Spectroscopy Study of Surface Films Formed on Li Electrodes Freshly Prepared in Alkyl Carbonate Solutions. *Langmuir* **1999**, *15* (9), 3334–3342.

(17) Huang, W.; Attia, P. M.; Wang, H.; Renfrew, S. E.; Jin, N.; Das, S.; Zhang, Z.; Boyle, D. T.; Li, Y.; Bazant, M. Z.; et al. Evolution of the Solid-Electrolyte Interphase on Carbonaceous Anodes Visualized by Atomic-Resolution Cryogenic Electron Microscopy. *Nano Lett.* **2019**, *19* (8), 5140–5148.

(18) Wang, X.; Zhang, M.; Alvarado, J.; Wang, S.; Sina, M.; Lu, B.; Bouwer, J.; Xu, W.; Xiao, J.; Zhang, J. G.; et al. New Insights on the Structure of Electrochemically Deposited Lithium Metal and Its Solid Electrolyte Interphases via Cryogenic TEM. *Nano Lett.* **2017**, *17* (12), 7606–7612.

(19) Hou, C.; Han, J.; Liu, P.; Yang, C.; Huang, G.; Fujita, T.; Hirata, A.; Chen, M. Operando Observations of SEI Film Evolution by Mass-Sensitive Scanning Transmission Electron Microscopy. *Adv. Energy Mater.* **2019**, *9* (45), 1–9.

(20) Nie, M.; Chalasani, D.; Abraham, D. P.; Chen, Y.; Bose, A.; Lucht, B. L. Lithium Ion Battery Graphite Solid Electrolyte Interphase Revealed by Microscopy and Spectroscopy.

J. Phys. Chem. C **2013**, *117* (3), 1257–1267.

(21) Jin, Y.; Kneusels, N. J. H.; Grey, C. P. NMR Study of the Degradation Products of Ethylene Carbonate in Silicon-Lithium Ion Batteries. *J. Phys. Chem. Lett.* **2019**, *10* (20), 6345–6350.

(22) Huff, L. A.; Tavassol, H.; Esbenshade, J. L.; Xing, W.; Chiang, Y.; Gewirth, A. A. Identi Fi Cation of Li-Ion Battery SEI Compounds through ^{7}Li and ^{13}C Solid-State MAS NMR Spectroscopy and MALDI-TOF Mass Spectrometry. *ACS Appl. Mater. Interfaces* **2016**, *8* (1), 371–380.

(23) Wang, L.; Menakath, A.; Han, F.; Wang, Y.; Zavalij, P. Y.; Gaskell, K. J.; Borodin, O.; Iuga, D.; Brown, S. P.; Wang, C.; et al. Identifying the Components of the Solid–Electrolyte Interphase in Li-Ion Batteries. *Nat. Chem.* **2019**, *11* (9), 789–796.

(24) Rikka, V. R.; Sahu, S. R.; Chatterjee, A.; Satyam, P. V.; Prakash, R.; Rao, M. S. R.; Gopalan, R.; Sundararajan, G. In Situ/Ex Situ Investigations on the Formation of the Mosaic Solid Electrolyte Interface Layer on Graphite Anode for Lithium-Ion Batteries. *J. Phys. Chem. C* **2018**, *122* (50), 28717–28726.

(25) von Wald Cresce, A.; Russell, S. M.; Baker, D. R.; Gaskell, K. J.; Xu, K. In Situ and Quantitative Characterization of Solid Electrolyte Interphases. *Nano Lett.* **2014**, *14* (3), 1405–1412.

(26) Rezvani, S. J.; Nobili, F.; Gunnella, R.; Ali, M.; Tossici, R.; Passerini, S.; Di Cicco, A. SEI Dynamics in Metal Oxide Conversion Electrodes of Li-Ion Batteries. *J. Phys. Chem. C* **2017**, *121* (47), 26379–26388.

(27) Liu, Z.; Lu, P.; Zhang, Q.; Xiao, X.; Qi, Y.; Chen, L. Q. A Bottom-Up Formation Mechanism of Solid Electrolyte Interphase Revealed by Isotope-Assisted Time-of-Flight Secondary Ion Mass Spectrometry. *J. Phys. Chem. Lett.* **2018**, *9* (18), 5508–5514.

(28) Huang, W.; Boyle, D. T.; Li, Y.; Li, Y.; Pei, A.; Chen, H.; Cui, Y. Nanostructural and Electrochemical Evolution of the Solid-Electrolyte Interphase on CuO Nanowires Revealed by Cryogenic-Electron Microscopy and Impedance Spectroscopy. *ACS Nano* **2019**, *13* (1), 737–744.

(29) Lu, P.; Harris, S. J. Lithium Transport within the Solid Electrolyte Interphase. *Electrochem. commun.* **2011**, *13* (10), 1035–1037.

(30) Ilott, A. J.; Jerschow, A. Probing Solid-Electrolyte Interphase (SEI) Growth and Ion

Permeability at Undriven Electrolyte-Metal Interfaces Using 7Li NMR. *J. Phys. Chem. C* **2018**, *122* (24), 12598–12604.

(31) Li, Q.; Lu, D.; Zheng, J.; Jiao, S.; Luo, L.; Wang, C. M.; Xu, K.; Zhang, J. G.; Xu, W. Li^+-Desolvation Dictating Lithium-Ion Battery's Low-Temperature Performances. *ACS Appl. Mater. Interfaces* **2017**, *9* (49), 42761–42768.

(32) Raguette, L.; Jorn, R. Ion Solvation and Dynamics at Solid Electrolyte Interphases : A Long Way from Bulk ? *J. Phys. Chem. C* **2018**, *122* (6), 3219–3232.

(33) Yildirim, H.; Kinaci, A.; Chan, M. K. Y.; Greeley, J. P. First-Principles Analysis of Defect Thermodynamics and Ion Transport in Inorganic SEI Compounds: LiF and NaF. *ACS Appl. Mater. Interfaces* **2015**, *7* (34), 18985–18996.

(34) Iddir, H.; Curtiss, L. A. Li Ion Diffusion Mechanisms in Bulk Monoclinic Li_2CO_3 Crystals from Density Functional Studies. *J. Phys. Chem. C* **2010**, *114* (48), 20903–20906.

(35) Shi, S.; Qi, Y.; Li, H.; Hector, L. G. Defect Thermodynamics and Diffusion Mechanisms in Li_2CO_3 and Implications for the Solid Electrolyte Interphase in Li-Ion Batteries. *J. Phys. Chem. C* **2013**, *117* (17), 8579–8593.

(36) Shi, S.; Lu, P.; Liu, Z.; Qi, Y.; Hector, L. G.; Li, H.; Harris, S. J. Direct Calculation of Li-Ion Transport in the Solid Electrolyte Interphase. *J. Am. Chem. Soc.* **2012**, *134* (37), 15476–15487.

(37) Ramasubramanian, A.; Yurkiv, V.; Foroozan, T.; Ragone, M.; Shahbazian-Yassar, R.; Mashayek, F. Lithium Diffusion Mechanism through Solid-Electrolyte Interphase in Rechargeable Lithium Batteries. *J. Phys. Chem. C* **2019**, *123* (16), 10237–10245.

(38) Zhang, Q.; Pan, J.; Lu, P.; Liu, Z.; Verbrugge, M. W.; Sheldon, B. W.; Cheng, Y. T.; Qi, Y.; Xiao, X. Synergetic Effects of Inorganic Components in Solid Electrolyte Interphase on High Cycle Efficiency of Lithium Ion Batteries. *Nano Lett.* **2016**, *16* (3), 2011–2016.

(39) Nikitina, V. A. Charge Transfer Processes in the Course of Metal-Ion Electrochemical Intercalation. *Curr. Opin. Electrochem.* **2020**, *19*, 71–77.

(40) Keefe, A. S.; Buteau, S.; Hill, I. G.; Dahn, J. R. Temperature Dependent EIS Studies Separating Charge Transfer Impedance from Contact Impedance in Lithium-Ion Symmetric Cells. *J. Electrochem. Soc.* **2019**, *166* (14), A3272–A3279.

(41) Tatara, R.; Karayaylali, P.; Yu, Y.; Zhang, Y.; Giordano, L.; Maglia, F.; Jung, R.; Schmidt, J. P.; Lund, I.; Shao-Horn, Y. The Effect of Electrode-Electrolyte Interface on

the Electrochemical Impedance Spectra for Positive Electrode in Li-Ion Battery. *J. Electrochem. Soc.* **2019**, *166* (3), A5090–A5098.

(42) Abe, T.; Sagane, F.; Ohtsuka, M.; Iriyama, Y.; Ogumi, Z. Lithium-Ion Transfer at the Interface Between Lithium-Ion Conductive Ceramic Electrolyte and Liquid Electrolyte-A Key to Enhancing the Rate Capability of Lithium-Ion Batteries. *J. Electrochem. Soc.* **2005**, *152* (11), A2151.

(43) Xu, K.; von Wald Cresce, A.; Lee, U. Differentiating Contributions to "Ion Transfer" Barrier from Interphasial Resistance and Li+ Desolvation at Electrolyte/Graphite Interface. *Langmuir* **2010**, *26* (13), 11538–11543.

(44) Yamada, Y.; Iriyama, Y.; Abe, T.; Ogumi, Z. Kinetics of Lithium Ion Transfer at the Interface between Graphite and Liquid Electrolytes: Effects of Solvent and Surface Film. *Langmuir* **2009**, *25* (21), 12766–12770.

(45) Jow, T. R.; Marx, M. B.; Allen, J. L. Distinguishing Li^+ Charge Transfer Kinetics at NCA⁄Electrolyte and Graphite⁄Electrolyte Interfaces, and NCA⁄Electrolyte and LFP⁄Electrolyte Interfaces in Li-Ion Cells. *J. Electrochem. Soc.* **2012**, *159* (5), A604–A612.

(46) Abe, T.; Fukuda, H.; Iriyama, Y.; Ogumi, Z. Solvated Li-Ion Transfer at Interface Between Graphite and Electrolyte. *J. Electrochem. Soc.* **2004**, *151* (8), A1120.

(47) Rodrigues, M. T. F.; Lin, X.; Gullapalli, H.; Grinstaff, M. W.; Ajayan, P. M. Rate Limiting Activity of Charge Transfer during Lithiation from Ionic Liquids. *J. Power Sources* **2016**, *330*, 84–91.

(48) Ishihara, Y.; Miyazaki, K.; Fukutsuka, T.; Abe, T. Kinetics of Lithium-Ion Transfer at the Interface between $Li_4Ti_5O_{12}$ Thin Films and Organic Electrolytes. *ECS Electrochem. Lett.* **2014**, *3* (8), A83–A86.

(49) Steinhauer, M.; Risse, S.; Wagner, N.; Friedrich, K. A. Investigation of the Solid Electrolyte Interphase Formation at Graphite Anodes in Lithium-Ion Batteries with Electrochemical Impedance Spectroscopy. *Electrochim. Acta* **2017**, *228*, 652–658.

(50) Hao, F.; Liu, Z.; Balbuena, P. B.; Mukherjee, P. P. Mesoscale Elucidation of Solid Electrolyte Interphase Layer Formation in Li-Ion Battery Anode. *J. Phys. Chem. C* **2017**, *121* (47), 26233–26240.

(51) Wang, A.; Kadam, S.; Li, H.; Shi, S.; Qi, Y. Review on Modeling of the Anode Solid

Electrolyte Interphase (SEI) for Lithium-Ion Batteries. *npj Comput. Mater.* **2018**, *4*, 15.

(52) Kim, S.-P.; Duin, A. C. T. Van; Shenoy, V. B. Effect of Electrolytes on the Structure and Evolution of the Solid Electrolyte Interphase (SEI) in Li-Ion Batteries: A Molecular Dynamics Study. *J. Power Sources* **2011**, *196* (20), 8590–8597.

(53) Leung, K.; Budzien, J. L. *Ab Initio* Molecular Dynamics Simulations of the Initial Stages of Solid-Electrolyte Interphase Formation on Lithium Ion Battery Graphitic Anodes. *Phys. Chem. Chem. Phys.* **2010**, *12* (25), 6583–6586.

(54) Marzouk, A.; Ponce, V.; Benitez, L.; Soto, F. A.; Hankins, K.; Seminario, J. M.; Balbuena, P. B.; El-Mellouhi, F. Unveiling the First Nucleation and Growth Steps of Inorganic Solid Electrolyte Interphase Components. *J. Phys. Chem. C* **2018**, *122* (45), 25858–25868.

(55) Fujie, T.; Takenaka, N.; Suzuki, Y.; Nagaoka, M. Red Moon Methodology Compatible with Quantum Mechanics/Molecular Mechanics Framework: Application to Solid Electrolyte Interphase Film Formation in Lithium-Ion Battery System. *J. Chem. Phys.* **2018**, *149* (4), 044113.

(56) Chen, Y. C.; Ouyang, C. Y.; Song, L. J.; Sun, Z. L. Electrical and Lithium Ion Dynamics in Three Main Components of Solid Electrolyte Interphase from Density Functional Theory Study. *J. Phys. Chem. C* **2011**, *115* (14), 7044–7049.

(57) Borodin, O.; Bedrov, D. Interfacial Structure and Dynamics of the Lithium Alkyl Dicarbonate SEI Components in Contact with the Lithium Battery Electrolyte. *J. Phys. Chem. C* **2014**, *118* (32), 18362–18371.

(58) Borodin, O.; Zhuang, G. V.; Ross, P. N.; Xu, K. Molecular Dynamics Simulations and Experimental Study of Lithium Ion Transport in Dilithium Ethylene Dicarbonate. *J. Phys. Chem. C* **2013**, *117* (15), 7433–7444.

(59) Bedrov, D.; Borodin, O.; Hooper, J. B. Li^+ Transport and Mechanical Properties of Model Solid Electrolyte Interphases (SEI): Insight from Atomistic Molecular Dynamics Simulations. *J. Phys. Chem. C* **2017**, *121* (15), 16098–16109.

(60) Muralidharan, A.; Chaudhari, M. I.; Pratt, L. R.; Rempe, S. B. Molecular Dynamics of Lithium Ion Transport in a Model Solid Electrolyte Interphase. *Sci. Rep.* **2018**, *8*, 10736.

(61) Li, Y.; Qi, Y. Energy Landscape of the Charge Transfer Reaction at the Complex Li/SEI/Electrolyte Interface. *Energy Environ. Sci.* **2019**, *12* (4), 1286–1295.

(62) Boyer, M. J.; Vilčiauskas, L.; Hwang, G. S. Structure and Li^+ Transport in a Mixed Carbonate / $LiPF_6$ Electrolyte near Graphite Electrode Surfaces : A Molecular Dynamics Study. *Phys. Chem. Chem. Phys.* **2016**, *18*, 27868–27876.

(63) Ohba, N.; Ogata, S.; Asahi, R. Hybrid Quantum-Classical Simulation of Li Ion Dynamics and the Decomposition Reaction of Electrolyte Liquid at a Negative-Electrode/Electrolyte Interface. *J. Phys. Chem. C* **2019**, *123* (15), 9673–9679.

(64) Haruyama, J.; Ikeshoji, T.; Otani, M. Analysis of Lithium Insertion / Desorption Reaction at Interfaces between Graphite Electrodes and Electrolyte Solution Using Density Functional + Implicit Solvation Theory. *J. Phys. Chem. C* **2018**, *122* (18), 9804–9810.

(65) Bhandari, A.; Gupta, P. K.; Bhattacharya, J.; Pala, R. G. S. Higher Energy Barrier for Interfacial Li-Ion Transfer from EC/$LiPF_6$ Electrolyte into (010) $LiFePO_4$ Cathode Surface than Bulk Li-Ion Diffusion within Both Cathode and Electrolyte. *J. Electrochem. Soc.* **2019**, *166* (13), A2966–A2972.

(66) Jorn, R.; Kumar, R.; Abraham, D. P.; Voth, G. A. Atomistic Modeling of the Electrode−Electrolyte Interface in Li-Ion Energy Storage Systems: Electrolyte Structuring. *J. Phys. Chem. C* **2013**, *117* (8), 3747–3761.

(67) Plimpton, S. Fast Parallel Algorithms for Short-Range Molecular Dynamics. *J. Comput. Phys.* 1995, pp 1–19.

(68) Martínez, L.; Andrade, R.; Birgin, E. G.; Martínez, J. M. Packmol: A Package for Building Initial Configurations for Molecular Dynamics Simulations. *J. Comput. Chem.* **2009**, *30*, 2157–2164.

(69) Fiorin, G.; Klein, M. L.; Hénin, J. Using Collective Variables to Drive Molecular Dynamics Simulations. *Mol. Phys.* **2013**, *111* (22–23), 3345–3362.

(70) Grossfield, A. WHAM: an implementation of the weighted histogram analysis method http://membrane.urmc.rochester.edu/content/wham (accessed Apr 1, 2020).

(71) Attia, P. M.; Das, S.; Harris, S. J.; Bazant, M. Z.; Chueh, W. C. Electrochemical Kinetics of SEI Growth on Carbon Black: Part I. Experiments. *J. Electrochem. Soc.* **2019**, *166* (4), E97–E106.

(72) Harris, O. C.; Tang, M. H. Molecular Probes Reveal Chemical Selectivity of the Solid-Electrolyte Interphase. *J. Phys. Chem. C* **2018**, *122* (36), 20632–20641.

(73) Borodin, O.; Smith, G. D. Quantum Chemistry and Molecular Dynamics Simulation Study

of Dimethyl Carbonate: Ethylene Carbonate Electrolytes Doped with $LiPF_6$. *J. Phys. Chem. B* **2009**, *113* (6), 1763–1776.

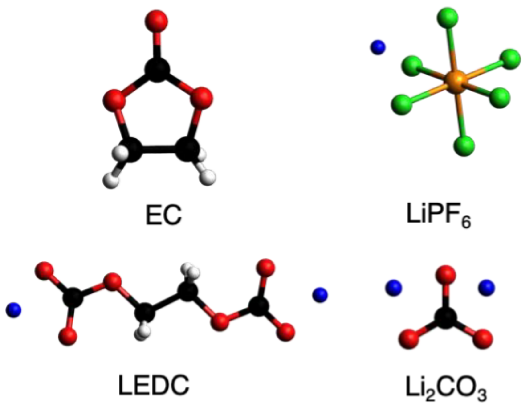

Figure 1. Molecular structures are shown for the electrolyte and electrode components with carbon (black), oxygen (red), hydrogen (white), phosphorous (orange), fluorine (green), and lithium (blue) shown in a ball-and-stick representation.

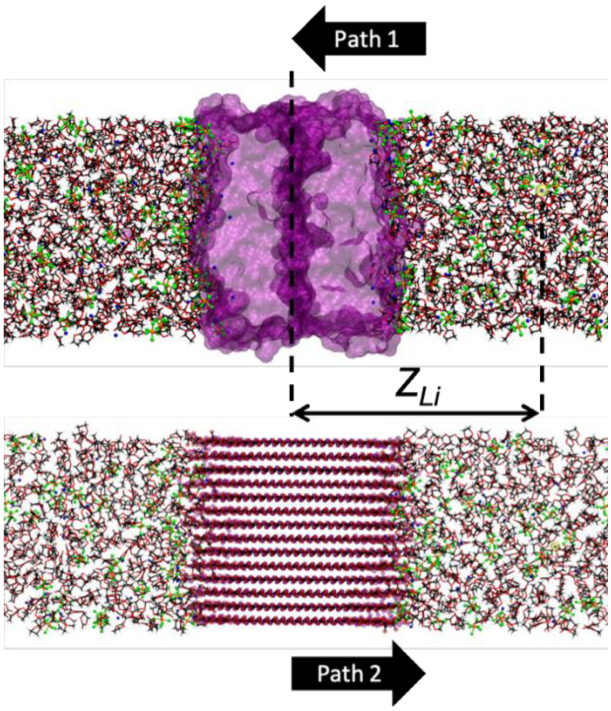

Figure 2. Snapshots are shown of the simulation cells used to model lithium ion insertion into an SEI comprised of amorphous Li_2EDC (top panel) and the [010] surface of crystalline Li_2CO_3 (bottom panel). The collective variable used in the umbrella sampling is shown, Z_{Li}, and the one-dimensional paths for ion insertion (Path 1) and extraction (Path 2) are indicated.

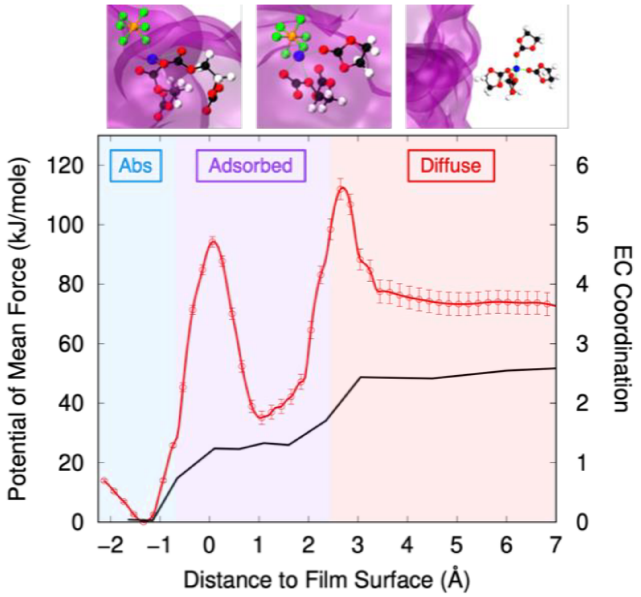

Figure 3. The potential of mean force for Path 1 (see Figure 2) at the LEDC film (red curve) correlated with changes in EC solvation (black curve). The shaded regions correspond to the defined segments of the lithium concentration profile based on EC coordination number. The EC curve has been scaled by 1.5 for clarity of presentation (see Figure 4 for unscaled numbers). Snapshots of the solvation shell surrounding the lithium are shown (left to right) at distances of -1.40, 1.35, and 12.00 Å, respectively, from the film surface. The color coding for the snapshots follows Figure 1 with the addition of the non-coordinating SEI groups shown as a purple surface. Only the first solvation shell for the lithium ion is shown for clarity.

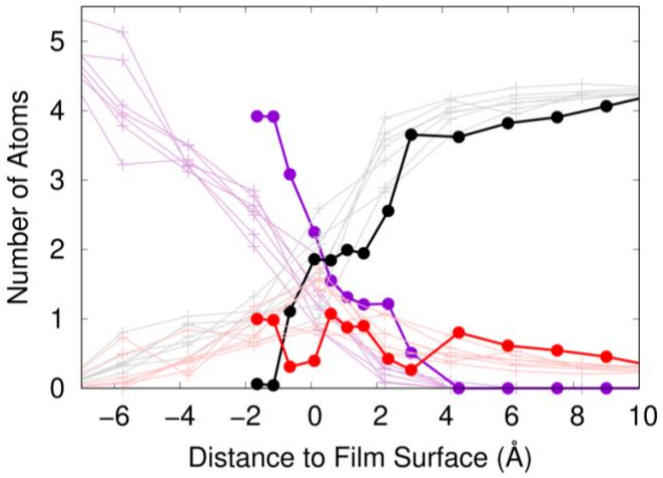

Figure 4. Plots of the coordination for the constrained lithium ion for Path 1 at the LEDC/electrolyte interface (bold lines and solid circles) and the averages across all lithium ions from the umbrella sampling simulations (light lines and crosses). The graph shows the coordination numbers for EC (black), PF_6^- (red), and surface carbonate groups from LEDC (purple).

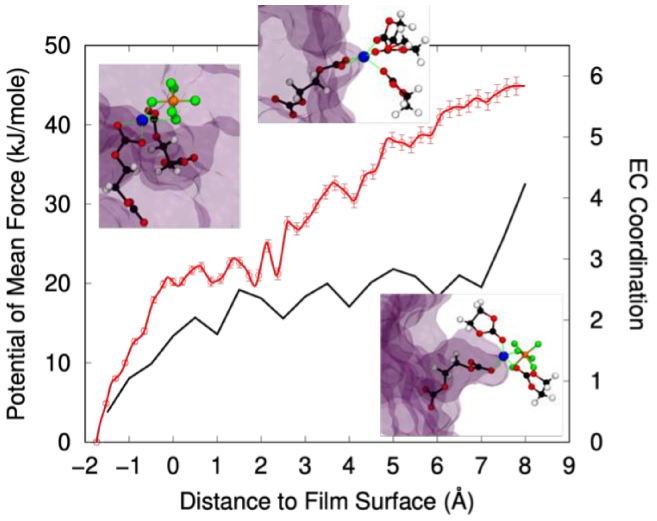

Figure 5. The potential of mean force for pulling a lithium ion from the LEDC film to the bulk electrolyte (red curve), according to Path 2 (see Figure 2), correlated to changes in EC solvation (black curve). Snapshots of the solvation shell surrounding the lithium are shown at distances of -0.75, 4.25, and 6.75 Å from the film surface and only the first solvation shell for the lithium ion is shown for clarity.

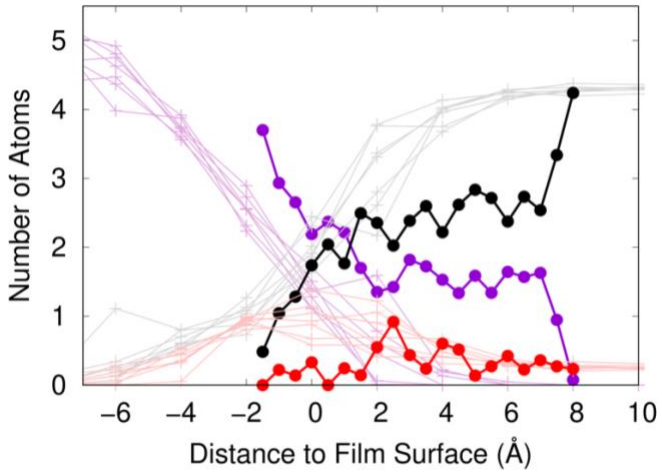

Figure 6. Plots of the coordination for the constrained lithium ion for Path 2 with LEDC (bold lines and solid circles) and the averages across all lithium ions from the umbrella sampling simulations (light lines and crosses) as a function of distance from the SEI. The graph shows the coordination numbers for EC (black), PF_6^- (red), and surface carbonate groups from LEDC (purple).

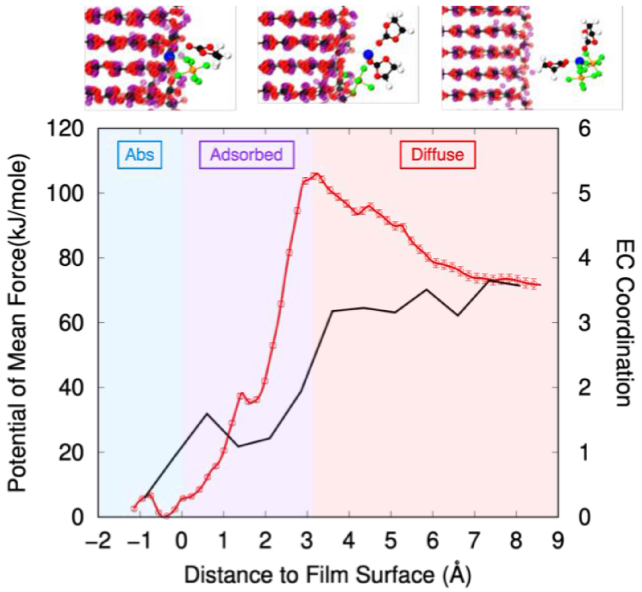

Figure 7. The potential of mean force for pulling a lithium ion from the Li_2CO_3 film into the bulk electrolyte (red curve) correlated to changes in EC solvation (black curve). Snapshots of the solvation shell surrounding the lithium are shown at distances of -2.0, 1.5, and 6.0 Å from the film surface following the same color convention in Figure 2, except the lithium carbonate crystal is now shown in a ball-and-stick representation rather than a purple surface plot. Only the first solvation shell for the lithium ion is shown for clarity and regions of the lithium density profile are indicated by shading according to definitions (see text).

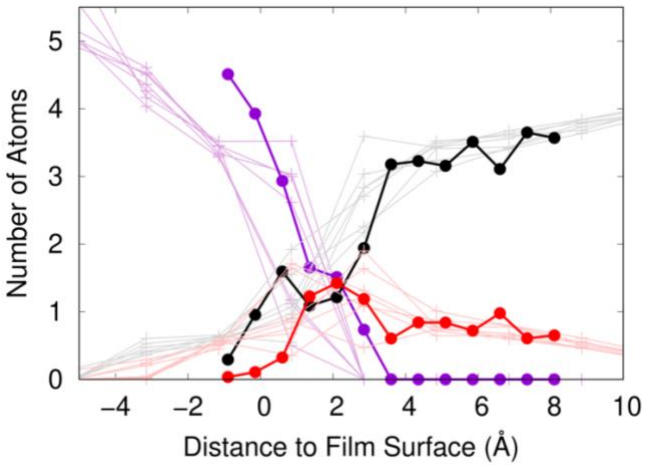

Figure 8. Plots of the coordination for the constrained lithium ion for Path 2 with Li_2CO_3 (bold lines and solid circles) and the averages across all lithium ions from the umbrella sampling simulations (light lines and crosses) as a function of distance from the SEI. The graph shows the coordination numbers for EC (black), PF_6^- (red), and surface carbonate groups from Li_2CO_3 (purple).

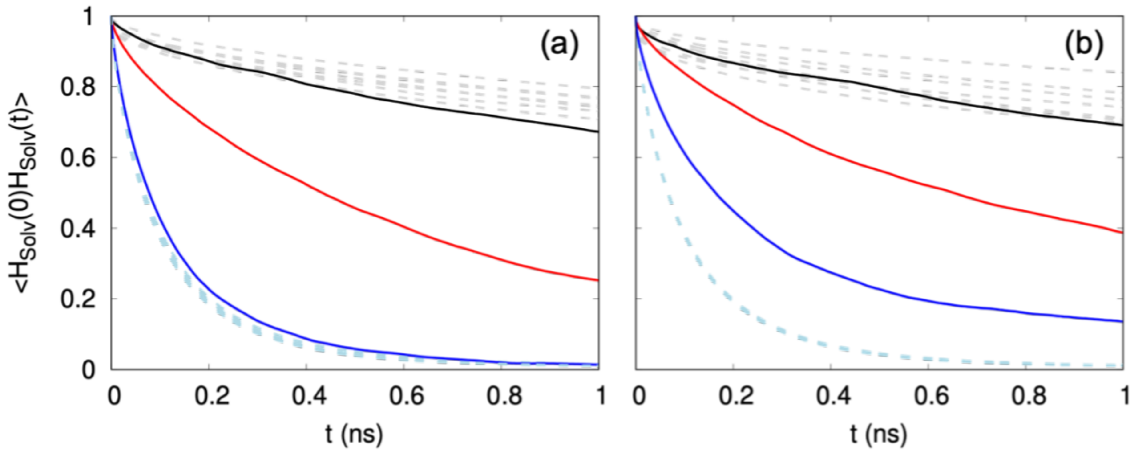

Figure 9. Plots of the solvation correlation function for EC coordinated to the constrained lithium (solid lines) and averaged across all lithium ions as a function of distance from the LEDC interface (dashed lines) for (a) Path 1 and (b) Path 2. Comparison is shown for the lithium constrained to distances of 0 (black), 4 (red), and 8 (blue) Å from the SEI surface and representative averages from six of the 40 window simulations are shown for the absorbed (black dashed) and bulk (blue dashed) electrolyte regions.

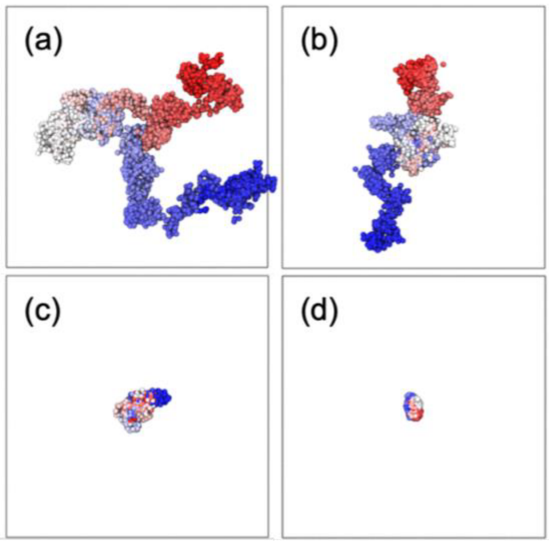

Figure 10. Trajectories from simulations of the constrained lithium ion over a 2.5 nanosecond interval from Path 1 at LEDC for distances of (a) 10.0, (b) 6.3, (c) 5.1, and (d) 2.6 Å from the SEI surface. The color of the bead corresponds to the timestamp of the lithium at the indicated position with blue corresponding to the beginning of the trajectory segment and red the end of the trajectory segment. The boundaries of the periodic simulation cell in the xy plane are shown in grey for perspective.

TOC Graphic